AFRL-AFOSR-UK-TR-2013-0023

Analytical and Experimental Characterization of Thick-Section Fiber-Metal Laminates

Dr. Rene Alderliesten
Greg Rickerd

Technische Universiteit Delft
TU Delft
Stevinweg 1
Delft 2628 CN Netherlands

EOARD Grant 11-3064

Report Date: June 2013

Final Report from 1 September 2011 to 30 November 2012

Air Force Research Laboratory
Air Force Office of Scientific Research
European Office of Aerospace Research and Development
Unit 4515 Box 14, APO AE 09421

REPORT DOCUMENTATION PAGE

Form Approved OMB No. 0704-0188

1. REPORT DATE *(DD-MM-YYYY)*	2. REPORT TYPE	3. DATES COVERED *(From – To)*
12 June 2013	Final Report	1 September 2011 – 30 November 2012

4. TITLE AND SUBTITLE

Analytical and Experimental Characterization of Thick-Section Fiber-Metal Laminates

5a. CONTRACT NUMBER

FA8655-11-1-3064

5b. GRANT NUMBER

Grant 11-3064

5c. PROGRAM ELEMENT NUMBER

61102F

6. AUTHOR(S)

Dr. Rene Alderliesten
Greg Rickerd

5d. PROJECT NUMBER

5d. TASK NUMBER

5e. WORK UNIT NUMBER

7. PERFORMING ORGANIZATION NAME(S) AND ADDRESS(ES)

Technische Universiteit Delft
TU Delft
Stevinweg 1
Delft 2628 CN Netherlands

8. PERFORMING ORGANIZATION REPORT NUMBER

N/A

9. SPONSORING/MONITORING AGENCY NAME(S) AND ADDRESS(ES)

EOARD
Unit 4515
APO AE 09421-4515

10. SPONSOR/MONITOR'S ACRONYM(S)

AFRL/AFOSR/IOE (EOARD)

11. SPONSOR/MONITOR'S REPORT NUMBER(S)

AFRL-AFOSR-UK-TR-2013-0023

12. DISTRIBUTION/AVAILABILITY STATEMENT

Distribution A: Approved for public release; distribution is unlimited. Government Purpose Rights

13. SUPPLEMENTARY NOTES

GOVERNMENT PURPOSE RIGHTS

14. ABSTRACT

Classical laminate theory, used in conjunction with the Ramberg-Osgood method (accounts for plastic deformation), is a powerful tool for the determination of numerous static properties of fiber metal laminates. However, the method runs into limitations if the laminate is loaded in a direction other than one parallel to the fibers. This limitation necessitates a more robust method, able to fully account for fibers oriented at angles other than 0 deg and 90 deg as well as plastic deformation at an angle other than the rolling or transverse directions of the metal sheets. Various methods were investigated regarding plastic deformation of the metal layers. While each method was shown to be fairly accurate, the method chosen for this project uses a von Mises yield criterion and applies kinematic hardening to determine the stiffness of individual metal layers as loading increases. The off-axis deformation properties of the prepreg layers were modeled by using equivalent constraint models where the layer of interest is explicitly modeled and the adjacent, constraining layers are modeled as equivalent, smeared layers. Using this method the degraded stiffness of the prepreg layer is found. At each loading step the stiffness properties of individual layers are calculated. These individual stiffnesses are then combined using the standard CLT method, thereby providing the laminate stiffness matrix. While the model accurately predicts stress-strain curves on-axis, additional work is needed to study the local interactions between metal and prepreg layers as damage occurs in each layer.

15. SUBJECT TERMS

EOARD, fiber-metal laminates, thick-section, composite materials

16. SECURITY CLASSIFICATION OF:			17. LIMITATION OF ABSTRACT	18, NUMBER OF PAGES	19a. NAME OF RESPONSIBLE PERSON
a. REPORT	b. ABSTRACT	c. THIS PAGE			Matthew Snyder, Maj, USAF
UNCLAS	UNCLAS	UNCLAS	SAR	36	**19b. TELEPHONE NUMBER** *(Include area code)* +44 (0)1895 616420

FA8655-11-1-3064 Final Report

Dr. R.C. Alderliesten, Technische Universiteit Delft
G.S. Rickerd, formerly of Technische Universiteit Delft

This material is based on research sponsored by the Air Force Research Laboratory, under agreement number FA8655-11-1-3064. The U.S. Government is authorized to reproduce and distribute reprints for Governmental purposes notwithstanding any copyright notation thereon.

Contents

List of Figures

List of Tables

Chapter 1

Summary

The purpose of this project was to develop a generalized stress-strain and failure model for fiber metal laminates. Models are available in the literature for tensile loading in the direction of the fibers but an adequate model does not exist for loading in other directions. The model developed in this research project predicts tensile stress-strain curves through failure at any in-plane loading angle for a generic laminate. The model individually models each layer of the laminate and predicts stiffness degradation as metal layers plastically deform and as prepreg layers experience transverse cracking in the matrix.

The model developed in this project works quite well for on-axis loading and moderately well for off-axis loading directions. Further research is still required to better understand the interactions between the metal and prepreg layers as cracks form in the matrix.

This model allows a further investigation of multi-axis loading as would be required to fully model multi-dimensional molding processes required to form laminates to complex geometries as would be required in the use of fiber metal laminates in aircraft wings.

Chapter 2

Introduction

2.1 Introduction

Fiber metal laminates (FML) are a class of material that combines the best properties of fibrous composites and monolithic metals into one material, while at the same time lessening some of the more undesirable properties of the constituents. This class of materials grew from the application of laminated metallic structures by post-World War II Fokker Aircraft. Laminated metallic structures were initially developed as an efficient method to tailor strength and stiffness in a structure to the local requirements, rather than the more traditional method of milling thick metal stock to the required dimensions. Testing and analysis showed that an added benefit of laminated metallic structures was improved fatigue properties due to a number of factors. One of these factors was that a crack must initiate separately for each individual metal layer. Meanwhile, the intact metal layers carry a significant portion of the load around the crack, thus reducing the stress intensity at the crack tip, and slowing the growth of the crack[20]. Additionally, the thinner sheet material has a higher fracture toughness and a lower crack growth rate than does thicker metallic sheet[17].

Laminated metallic structures were later improved by the addition of high strength fiber composites between the laminated metallic sheets, thus creating a material class generally known as fiber metal laminates, or FML. The addition of the fibrous layer further decreased the rate at which fatigue cracks grow through the structure. The first combination of metal and fiber to be studied extensively was known as ARALL and was a combination of Aramid fibers and either AL2024 or AL7075[20]. Certain disadvantages were discovered in the ARALL research process that led to a variant of ARALL that made use of glass fibers instead of Aramid fibers. This variant became known as GLARE, which stands for ***GLA****ss* ***RE****inforced aluminum*, and is thoroughly described in Roebroeks' thesis[16]. GLARE is the most heavily researched FML, and is a combination of AL2024-T3 and S2 glass fibers in an FM-94 epoxy adhesive[15].

2.2 Motivation

Extensive research is available in the open literature, covering virtually all strength, damage tolerance, and manufacturing aspects of FML structures. Much of the research was to develop analytical models for important mechanical and structural properties. These properties are understood so well that GLARE has been applied in the fuselage of the Airbus A380[2]. With the material certified for thin skin applications, researchers are now working on applying this material to structures requiring thick sheets, such as aircraft wings. Previous research on GLARE utilized aluminum sheets of between 0.3mm and 0.5mm in thickness and resulted in analytical and empirical models of static and fatigue properties that have been validated for GLARE sheets composed of these relatively thin sheets of

aluminum[1, 3, 5, 7, 9, 14, 18, 19]. One group of researchers has started to investigate GLARE sheets composed of aluminum layers greater than 1.0mm in thickness; however there has been no research to quantify material behavior in the interim range of 0.5mm to 1.0mm.

In addition to material property changes, thicker sheet applications of FML technology raise the possibility that structural and manufacturing issues may become driving factors in the design of thick sheet structures. Design aspects such as doublers and ply drop-offs that required minimal design effort when manufactured out of thin metallic sheets could pose significant design problems when manufactured out of thick metallic sheets.

In order to answer the questions raised above, it is necessary to develop a robust analytical model which is not limited in the number or thickness of aluminum sheets as well as one that is not limited by the loading angle. The use of GLARE in the fuselage of the A380 allows a very simple assumption, namely that the only loading applied to the FML sheet is confined to the longitudinal and circumferential directions of the fuselage. The A380 is designed so that fibers are aligned in the principal loading directions, and therefore a simple analytical or empirical model is sufficient. In order to use FML sheets in other loading scenarios an enhanced model is required that is able to calculate stress-strain and failure of generalized laminates at any loading angle.

2.3 Research Plan

The original goal of this research project was to answer all of the questions required before an aircraft wing could be manufactured of FML sheets. In the process of this project it became clear that this goal would be impossible to reach in the short timeframe of this grant. The reason for the difficulty was that the complexity of modelling an FML sheet at an angle other than along a fiber was much higher than was anticipated due to the damage that occurs in an off-axis FML sheet as it is loaded to failure, and the complex stiffness changes that occur in both the aluminum and fiber layers as the load is increased. Therefore, this project focused on developing a robust analytical model capable of capturing the damage state in an FML at a given load as well as the stiffness degradation due to that damage.

Chapter 3

Methods, Assumptions, and Procedures

Two main methods exist to determine material properties along the fiber direction in an FML. The first of these, the metal volume fraction (MVF) method, is essentially a rule of mixtures calculation using the material property of interest in each constituent scaled by the percentage of the laminate that is the constituent[14]. This method is quite accurate for calculating properties in fiber directions, but is not applicable at any other angle, and in fact is only able to predict the values of yield and ultimate strength, not the loading path to reach those values, and therefore it will not be discussed any further in this report.

The second method is the familiar classical lamination theory (CLT) method commonly used to calculate traditional composite material properties. Theoretically, this method is ideally suited for FML calculations at an off-axis angle because it is built deliberately to calculate properties at any loading angle. The problem found, as seen in Figure 3.1, in this project was that the plasticity of the aluminum layer is not the only damage affecting the laminate stiffness. In off-axis loading the prepreg layers exhibit a gradual decrease in stiffness that is unaccounted for in the standard CLT method, thus a stiffness degradation model is required for the composite layers loaded off-axis.

The big assumption used in this project is that the basic premise of the CLT method is valid with the plastic deformation present in aluminum layers, but must simply be accounted for in calculations. Under this assumption a plastic deformation model for the aluminum layers can be used. Simple methods such as the Ramberg-Osgood or secant modulus models for plastic deformation can be used. The problem with each of these methods is that they are both limited because each angle of loading requires a tensile stress-strain curve at that angle. A solution to this problem is through using a kinematic hardening model to predict plastic deformation properties of the aluminum layers in FMLs.

3.1 Plastic Deformation

In the case of loading only in the rolling or transverse directions simple one dimensional yield functions are sufficient to predict plastic deformation. In the case of off-axis loading a more complicated method is required to model plasticity.

Numerous methods are available to model plasticity in metals[13, 21]. The model that was chosen in this study was based on the von Mises yield function, but to account for anisotropic yielding and hardening of the aluminum constituent, the Prandtl-Reuss flow rule is applied, thus allowing shifting of the yield surface, but not a change in size or shape[4]. A series of linear hardening coefficients were determined from stress-strain curves. The linear nature of the hardening coefficients means that the

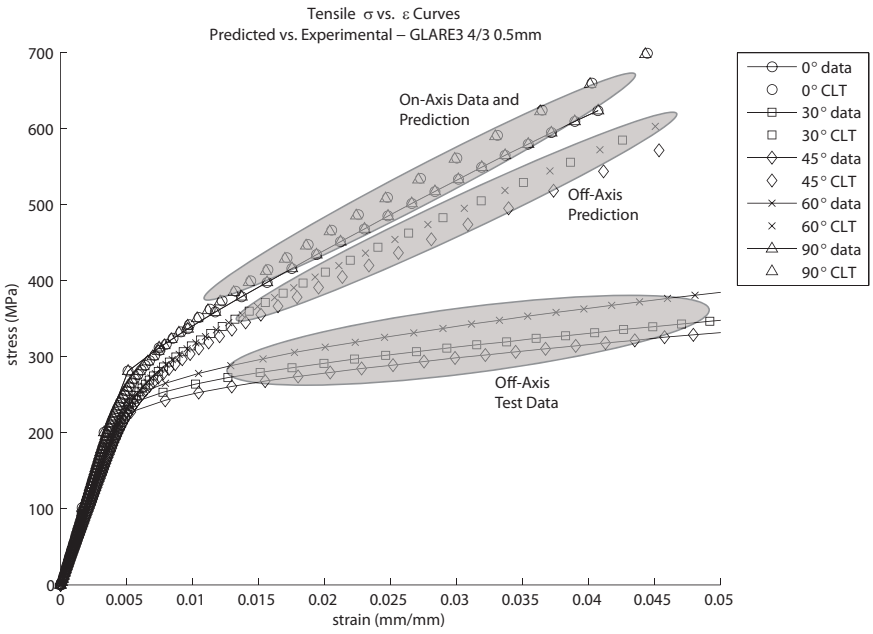

Figure 3.1 – *Stress-Strain Curves Predicted with CLT at various loading angles*

smooth hardening behavior present in aluminum is lost in the modelling. This factor can be mitigated by choosing strain intervals such that the linear representation of the stress-strain curve most closely matches the actual shape of the curve.

The standard plane stress von Mises yield function was chosen for this model,

$$\begin{aligned} f &= \sqrt{\overline{\sigma_x}^2 + \overline{\sigma_y}^2 + \overline{\sigma_x \sigma_y} + 3\overline{\tau_{xy}}^2} - \sigma_Y = 0 \\ f &= \sigma_e - \sigma_Y = 0 \end{aligned} \tag{3.1}$$

where the square root represents the effective stress applied to the material, σ_e and σ_Y is the yield stress of the metal. The variables $\overline{\sigma_{x/y}}$ and $\overline{\tau_{xy}}$ are defined as,

$$\begin{aligned} \overline{\sigma_x} &= \sigma_x - \alpha_x \\ \overline{\sigma_y} &= \sigma_y - \alpha_y \\ \overline{\tau_{xy}} &= \tau_{xy} - \alpha_{xy} \end{aligned}$$

where, the variables α_x, α_y, and α_{xy} are the offsets in stress space of the yield surface. The von Mises yield surface is used to determine the point in loading where plastic deformation begins. This occurs when the expression for f in Equation 3.1 equals zero. At this point, assuming the effective stress has not exceeded the ultimate strength of the metal, plastic deformation occurs. The Prandtl-Reuss flow rule states that plastic flow occurs perpendicular to the yield surface, and can be described using an associative flow rule such as,

$$\dot{\epsilon_p} = \Delta\lambda \frac{\partial f}{\partial \sigma} \tag{3.2}$$

where $\dot{\epsilon_p}$ is the plastic strain rate and $\Delta\lambda$ is the plastic strain rate multiplier. One requirement of the Prandtl-Reuss flow rule is that as yielding occurs the stress state always stays on the yield surface, meaning that the effective stress is always less than or equal to the yield stress, $\sigma_e \leq \sigma_Y$.

By definition, the stress state, f, can not be greater than zero, and by convention it is assumed that the plastic strain occurs in a positive manner, therefore λ will be greater than or equal to zero. If no plastic flow occurs, the plastic strain rate, $\dot{\epsilon_p} = 0$. So, if plastic flow does not occur when $f < 0$ and the only possible states are $f \leq 0$, it follows that plastic flow only occurs when $f = 0$.

Assuming that plastic flow occurs at a constant rate, $\dot{f} = 0$, the partial derivative of Equation 3.1 must equal zero,

$$\dot{f} = \frac{\partial f}{\partial \sigma} \{\Delta\sigma\} + \frac{\partial f}{\partial \alpha} \{\Delta\alpha\} = 0 \tag{3.3}$$

The partial differential, $\frac{\partial f}{\partial \sigma}$ is essentially the outward facing normal vector to the yield surface, while the second differential, $\frac{\partial f}{\partial \alpha}$ is the inward facing normal vector, the variable $\{\vec{n}\}$ and $-\left\{\vec{n}^T\right\}$ will be used to represent these differentials. Taking the differential, $\vec{n}^T$ is found to be,

$$\{\vec{n}\} = \frac{1}{2\sigma_e} \begin{Bmatrix} 2\overline{\sigma_x} - \overline{\sigma_y} \\ 2\overline{\sigma_y} - \overline{\sigma_x} \\ 6\overline{\tau_{xy}} \end{Bmatrix} \tag{3.4}$$

There are multiple methods to account for strain hardening. In this work a kinematic hardening model is used. A kinematic hardening model requires that the yield surface moves in stress space, but does not expand. This project uses a Ziegler yield surface evolution law,

$$\{\Delta\alpha\} = C_z \Delta\lambda \{\bar{\sigma}\} \tag{3.5}$$

where C_z is the hardening coefficient. The value obtained for $\{\Delta\alpha\}$ is then substituted back into Equation 3.1 for the next load increment. Plugging this equation for $\{\Delta\alpha\}$ into Equation 3.3 gives,

$$\left\{\vec{n}^T\right\} \{\Delta\sigma\} - C_z \Delta\lambda \sigma_e = 0 \tag{3.6}$$

For simplicity, a one dimensional case can be imagined.

$$\Delta\sigma_x = C_z \Delta\lambda \sigma_o \tag{3.7}$$

This equation can be further simplified if the hardening modulus is taken to be, $H = \frac{\partial \sigma_x}{\partial \epsilon_x}$, thus the Hardening coefficient, C_z is,

$$C_z = \frac{H}{\sigma_o} \tag{3.8}$$

The incremental stress change can be thought of as,

$$\{\Delta\sigma\} = [Q] \left(\{\Delta\epsilon_{tot}\} - \{\Delta\epsilon_{plastic}\}\right) \tag{3.9}$$

but the change in plastic strain can be described from Equation 3.2 to be $\Delta\lambda \{\vec{n}\}$, so this equation can be simplified to,

$$\{\Delta\sigma\} = \{\Delta\sigma_{elastic}\} - \Delta\lambda [Q] \{\vec{n}\} \tag{3.10}$$

This equation can be pictured as an assumed elastic stress step from the first term on the right, with a correction step to move the actual stress state back to the yield surface. This process is pictured in Figure 3.2.

By rearranging the definition of equivalent stress and making use of Equations 3.8 and 3.10, and labeling the assumed elastic stress state and kinematic shift variables as *trial* values the following equation is found,

$$\{\overline{\sigma_{n+1}}\} + \left(\{\alpha_{n+1}\}^{trial} + C_z \Delta\lambda \{\overline{\sigma_{n+1}}\}\right) = \{\sigma_{n+1}\}^{trial} - \Delta\lambda [Q] \{\vec{n}\} \tag{3.11}$$

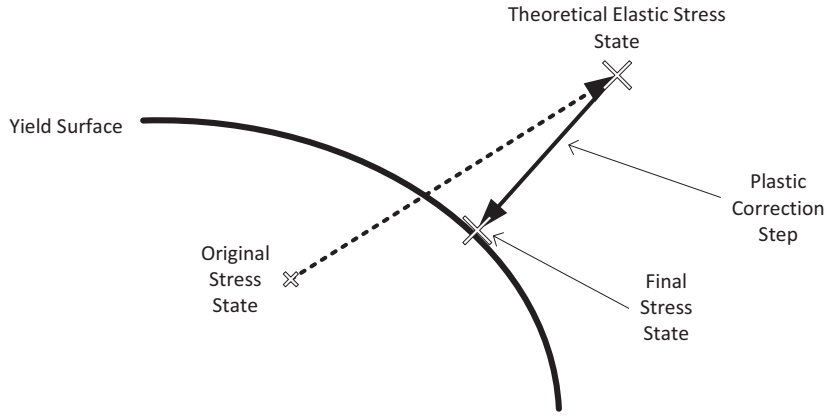

Figure 3.2 – *Elastic Step with a Plastic Corrector Step*

simplifying this equation using Equation 3.8 gives an equation relating the trial stress and the corrected stress,

$$\{\overline{\sigma_{n+1}}\}\left(1+\frac{H}{\sigma_{eC}}\Delta\lambda\right)=\{\overline{\sigma_{n+1}}\}^{trial}-\Delta\lambda\,[Q]\,\{\vec{n}\} \tag{3.12}$$

Substitution of $\Delta\lambda$ back into Equation 3.10 gives the stress state after the plastic corrector step. The plastic corrector step also causes a shift of the yield surface given by $\Delta\alpha$ from Equations 3.5 and 3.8. The stiffness degradation due to plasticity is found from Equations **??**

$$[Q]_{new}=[Q]_{old}\left([I]-\frac{\{\vec{n}\}\,\{\vec{n}\}^{T}\,[Q]_{old}}{\{\vec{n}\}^{T}\,[Q]_{old}\,\{\vec{n}\}+H'}\right) \tag{3.13}$$

3.2 Progressive Failure Theories in Composites

The CLT method performed quite well through the elastic portion of the stress strain curves, but once the matrix fractures the predicted curves begin to vary from test data. The most likely reason for this divergence is that when the matrix fails, it doesn't fail through the entire lamina, but rather at a single place. Due to the bridging nature of the adjacent laminae, the load carrying capacity lost at that fracture site is simply carried by the remaining laminae via a shear transfer as seen in Figure 3.3. After the first matrix failure and load transfer, a failure will occur at another location within the same lamina, possibly at the same load, but also possibly after additional load application. In this way, the stiffness loss due to matrix fracture is a gradual process, rather than a drop from full, undamaged stiffness to zero matrix stiffness[12].

The challenge lies in determining the distance over which the shear bypass acts before it disappears and the load it was transferring has returned to the cracked matrix layer. There are a couple of different methods to accomplish this stress analysis. For applicability to FML cracking a model must allow for both generic laminates, symmetric or asymetric, and generic loading, loading at other than 0° or 90°. Additionally the model must be built using generally known material properties such as modulus, Poisson's ratio, and fracture strengths in material orientations. This last point is important because

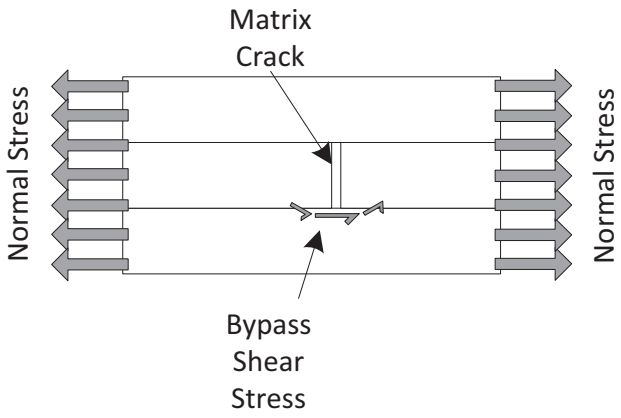

Figure 3.3 – *Transfer of Load Around a Matrix Crack*

it will limit the need to perform additional testing whenever a new orientation, new materials, or new geometry was required.

Progressive matrix damage is not a problem limited to FMLs loaded off-axis, but is also prevalent in a number of fiber composite laminates. Various researchers have investigated different methods to predict the evolution of the damage in these laminates. One method investigates the strain energy release rate in symmetric, balanced, cross-ply laminates where the majority of the fibers are oriented 90° to the load direction[10, 11]. This method performs well at predicting the progressive stiffness degradation of the matrix, but requires additional testing to determine the strain energy release rate of cross-ply laminates and was not proven out for angles other than 90° or for more than one crack in a matrix.

This method has also been extended to off-axis cracking such as would be found in the θ layers in a $[0°/\theta]_S$ laminate. This method is not applicable to general laminates due to the numerous layers not aligning with the central cracked layer as presented in this model.

The best method to model the complicated nature of an FML layup was proposed by Fan and Zhang[6]. This model uses equivalent contraint models (ECM) to create smeared constraining layers above and below an explicitly modeled cracked layer. These ECM layers are modeled as homogeneous layers which resist the opening of the crack. By modeling the adjacent layers in this way the model can be significantly simpler than explicitly modeling the constraining effect each layer has upon the cracked layer. This model also allows cracks in multiple layers by simply combining the degraded layer into the constraining layer. These ECM models are then used to calculate an in-situ damage effective function (IDEF) which can be used to describe the stiffness degradation of a composite layer due to matrix cracking in that layer.

In a laminate with multiple layers, the constraining effect of a layer upon another cracked layer decreases significantly the further it is away from the cracked layer[23]. For this reason the ECM model was modified from a 3-layer model as described above to a 5-layer model[22]. The 5-layer model differs by explicitly modeling layers directly adjacent to the cracked layer while modeling the remaining layers as homogenous layers.

3.2.1 In-Situ Damage Effective Functions

The coordinate system used to determine the IDEFs is the standard composite system where $x_1 - x_2 - x_3$ is the individual laminate system where 1 is along the fiber direction, 2 is perpendicular to the fiber, and 3 is out of the plane of the laminate. One of the assumptions required is the geometry of

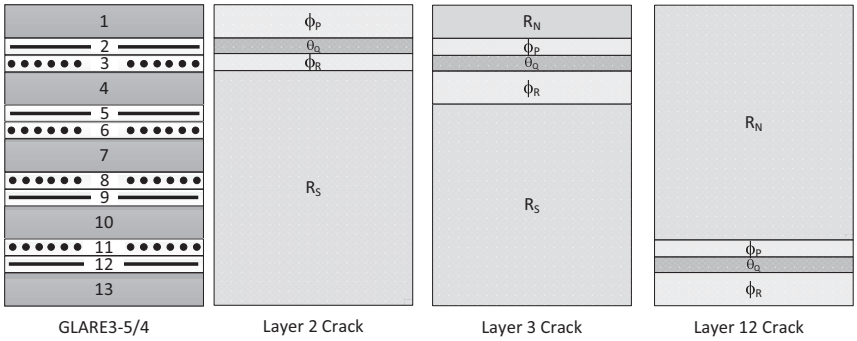

Figure 3.4 – *ECM laminates required for FML*

cracks within each lamina. The standard assumption used in predicting matrix cracking is that cracks are distributed evenly through the lamina in the x_2 direction, and continue the entire length of the specimen in the x_1 direction. The IDEFs are calculated using a stress averaging approach through the thickness of the laminate as described initially by Hill[**?**]. The IDEFs derived by Zhan and Herrmann are used to modify the stiffness matrix of an undamaged lamina, by the following equation,

$$\left[Q^k\right] = \begin{bmatrix} Q^0_{11} & Q^0_{12} & 0 \\ Q^0_{12} & Q^0_{22} & 0 \\ 0 & 0 & Q^0_{66} \end{bmatrix} - \begin{bmatrix} \frac{\left(Q^0_{12}\right)^2}{Q^0_{22}}\Lambda^k_{22} & Q^0_{12}\Lambda^k_{22} & 0 \\ Q^0_{12}\Lambda^k_{22} & Q^0_{22}\Lambda^k_{22} & 0 \\ 0 & 0 & Q^0_{66}\Lambda^k_{66} \end{bmatrix} \tag{3.14}$$

where Λ^k_{22} is the IDEF related to stiffness reduction in the tensile loading of the matrix and Λ^k_{66} is the IDEF related to stiffness reduction in the shear loading of the matrix. The value of these IDEFs are calculated from a stress-analysis of the cracked lamina.

3.2.2 Equivalent Constraint Models

Equivalent constraint models are built from the specific layups of the laminates to be analyzed. In a general composite laminate there are eight different ECM laminates that need to be described. In the case of FML sheets however, many of the ECM formulations are not needed as they do not exist in FML. For simplicity, the following notation will be used to describe the various layers in an ECM:

- R_N - Top homogeneous layer
- ϕ_P - Single layer above crack
- θ_Q - Cracked layer
- ϕ_R - Single layer below crack
- R_S - Bottom homogeneous layer

Because of the manner in which FML sheets are used in structures, prepreg plies are never used on the outer surfaces, eliminating four of the possible ECM laminates. Additionally, since at least four individual layers (two aluminum and two prepreg) are used in FML an additional ECM is eliminated, thus leaving only three possible ECM laminates for analysis. These three laminates are shown in Figure 3.4.

The equivalent constraint model is then applied individually for each cracked composite layer. The equilibrium and constitutive equations for each layer are found. Due to stress and displacement

continuity between adjacent cracked layers the equilibrium and constitutive equations for each layer are coupled and can be easily represented via a single matrix equation.

A number of simplifying relations can be used to aid in solving equilibrium and constitutive equations. First, the out-of-plane displacements of adjacent layers are constant, meaning the layers do not separate as load is applied. This simplification enables calculation of the the curvatures of the laminate. Secondly, the interfaces between laminae must have constant shear tractions on each face. And lastly, the top and bottom surfaces must be stress free. These last two facts lead to a matrix relationship between shear tractions at the interface and curvature of the laminate.

Looking at in-plane displacements instead of curvatures, a very similar process was followed, and a relation between displacements, curvatures, and interface shear stresses was determined. Combining these matrix equations gives a differential equation of the form,

$$[\Omega]\{\kappa\}_{,22} - [C]\{\kappa\} = \{0\} \tag{3.15}$$

where, $[\Omega]$ is a function of lamina geometry and extensional and bending stiffnesses, and $[C]$ is a function of shear extensional stiffness. The solution to this equation is

$$\left\{\kappa^{(k)}\right\} = \sum_{j=1}^{n} \left\{p_j^{(k)}\right\} F_j sinh\left(\lambda_j x_2\right) \tag{3.16}$$

where $\left\{p_j^{(k)}\right\}$ is the eigenvector found from the eigenvalues, (λ_j) and k is the number of the equivalent constraint layer. Using the curvatures $\left\{\kappa^{(k)}\right\}$, the midplane displacements of the laminate are found via integration. The force and moment equilibrium equations are then used for each equivalent layer, leaving two sets of constants to determine.

The constants in the force and moment equilibrium equations are determined using the relation between mid-plane displacements of the equivalent constraint layers and the curvatures of each of those laminates. Using displacement relationships, laminate boundary conditions, and force continuity at the crack faces leads to a series of five vector equations allowing for solution of the required constants.

Using the constants just determined, the stiffness degradation of a laminate due to a crack or cracks within individual layers can be found using in-situ damage effective functions (IDEF),

$$\begin{aligned} \Lambda_{22} &= \frac{h^{(II)}}{2} \sum_{j=1}^{10} p_{j2}^{(II)} \Phi_{j1}(s) \\ \Lambda_{66} &= \frac{h^{(II)}}{2} \sum_{j=1}^{10} p_{j6}^{(II)} \Phi_{j2}(s) \end{aligned} \tag{3.17}$$

where $p_{j2}^{(II)}$ and $p_{j6}^{(II)}$ are the values of the eigenvectors for each layer and $\Phi_{j1}(s)$ and $\Phi_{j2}(s)$ are the values of the constants just calculated. The IDEF are then used to degrade the stiffness of the cracked layer using Equation 3.14. This new value for the stiffness of the cracked layer, $[Q]$ is used in the determination of the laminate extensional stiffness matrix $[A]$ commonly used in the classical lamination theory. Full details can be found in Rickerd's thesis[13].

3.2.3 Full FML Model

The degradation models described in the previous sections enable a fully generic FML model which accounts for damage in both metal and composite layers. Degraded stiffness matrices for composite layers, Equation 3.14, and metallic layers, Equation 3.1, are combined in the standard classical laminate theory calculations of the $[ABD]$ matrix,

$$\left\{ \begin{array}{c} N \\ M \end{array} \right\} = \left[\begin{array}{c} AB \\ BD \end{array} \right] \left\{ \begin{array}{c} \epsilon_o \\ \kappa \end{array} \right\} \tag{3.18}$$

where,

$$\begin{aligned}
[A] &= \int_{-t/2}^{t/2} \left[\bar{Q}_{ij}\right] dz \\
&= \sum_{i=1}^{n_m} t_{m_i} \left[\bar{Q}_m\right] + \sum_{j=1}^{n_{pp}} t_{pp_j} \left[\bar{Q}_{pp}\right] \\
[B] &= \int_{-t/2}^{t/2} \left[\bar{Q}_{ij}\right] z dz \\
&= \left(\frac{1}{2}\right) \sum_{i=1}^{n_m} \left[\bar{Q}_m\right] \left(z_i^2 - z_{i-1}^2\right) + \frac{1}{2} \sum_{j=1}^{n_{pp}} \left[\bar{Q}_{pp}\right] \left(z_j^2 - z_{j-1}^2\right) \\
[D] &= \int_{-t/2}^{t/2} \left[\bar{Q}_{ij}\right] z^2 dz \\
&= \left(\frac{1}{3}\right) \sum_{i=1}^{n_m} \left[\bar{Q}_m\right] \left(z_i^3 - z_{i-1}^3\right) + \frac{1}{3} \sum_{j=1}^{n_{pp}} \left[\bar{Q}_{pp}\right] \left(z_j^3 - z_{j-1}^3\right)
\end{aligned} \tag{3.19}$$

and the $[Q]$ matrices are taken from the degraded stiffness matrices of individual layers. This method allows development of a full stress-strain curve under off-axis loading in FML materials.

Chapter 4

Results and Discussion

4.1 Off-Axis CLT Results

The previous sections have presented the methods used in this project to determine the stiffness degradation in fiber metal laminates due to plastic deformation of the metal layers and matrix cracking in the composite layers. This section shows the tensile stress-strain curves predicted using the CLT method and the previously described stiffness degradation models. Tensile stress strain data was used at 0°, 30°, 45°, 60°, and 90° to the aluminum rolling direction in GLARE3 4/3 0.5mm laminates. The comparisons between test data and predictions are shown in Figures 4.1-4.5

4.2 Discussion

The predicted stress-strain curves at 0°, Figure 4.1, and 90°, 4.5, match test data fairly well, but the predictions for off-axis angles, Figures 4.2-4.4 show considerable difference from test data in both general shape and failure strain. The following sections will discuss possible reasons for this variation as well as recommending a change to the model.

4.2.1 Yield Model

The yield function and hardening law used in this model assumed a single radius for the yield surface regardless of the loading orientation, and the material hardened at the same rate for any loading combination. These assumptions greatly simplified calculations, but it must be questioned whether they are accurate for general loading orientations.

Fibers in FML sheets cause very strong directionality effects, meaning that in fiber directions the stiffness is possibly 10% higher than at 45°. This directionality makes deformation in off-axis directions much easier than in fiber-directions. The yield model used in this project assumes that simply transforming stresses to the L/LT directions and applying the yield function accurately predicts stress-strain behavior of the laminate. This assumption appears to be insufficient to describe the off-axis tensile behavior above 2-4% strain. Further research is needed to determine whether the simple yield surface presented in Section 3.1 is sufficient to predict the off-axis yield behavior.

The effect of shifting of the yield surface in stress-space is entirely dependent upon the loading orientation of the specimen as well as the material data used to shift the surfaces. The shift data used by Bouwman[4] describes a moderately anisotropic material, where the offset in the rolling direction is over 50MPa greater than in the transverse direction. This drastic difference between the L and LT directions was not seen in this project, as can be seen in the stress-strain curves, Figures 4.6-4.9.

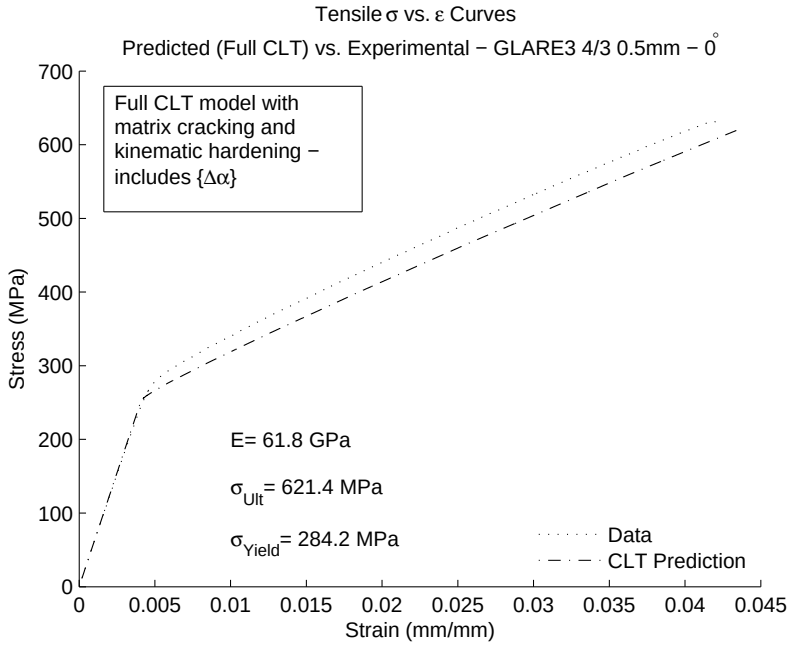

Figure 4.1 – *Full CLT Stress-Strain Prediction - 0° Specimen*

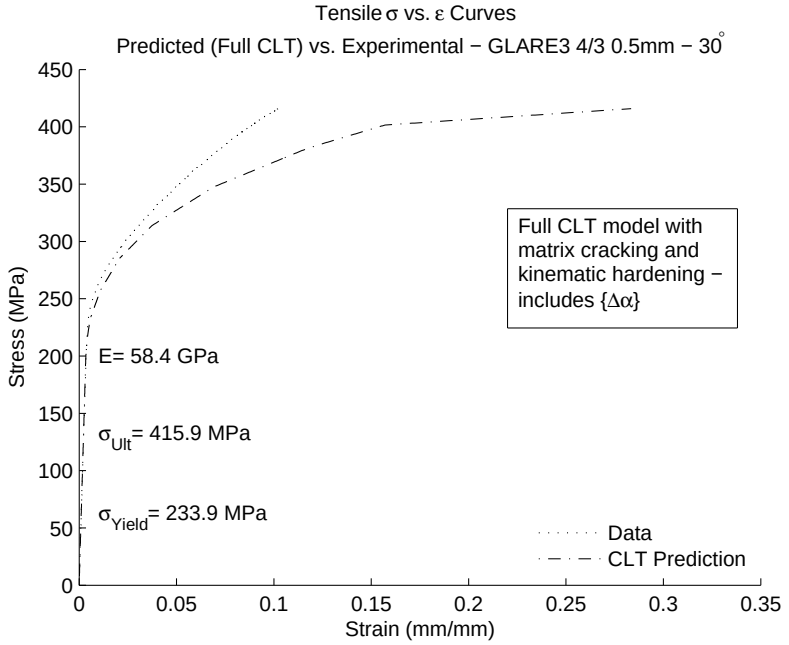

Figure 4.2 – *Full CLT Stress-Strain Prediction - 30° Specimen*

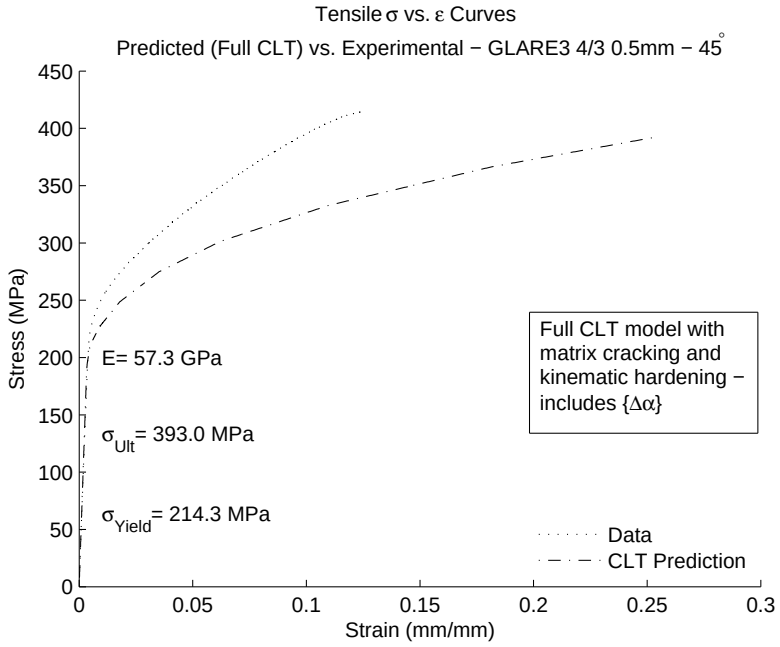

Figure 4.3 – *Full CLT Stress-Strain Prediction* - 45° *Specimen*

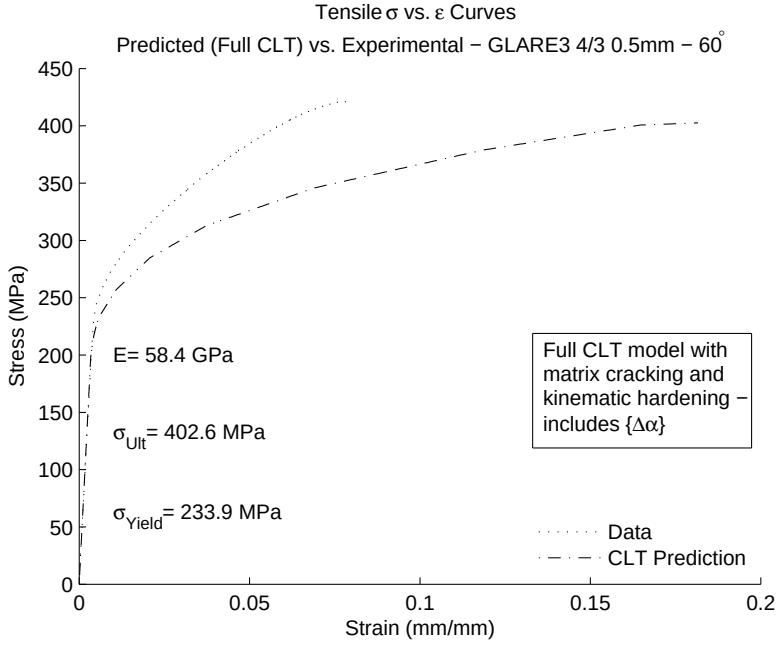

Figure 4.4 – *Full CLT Stress-Strain Prediction* - 60° *Specimen*

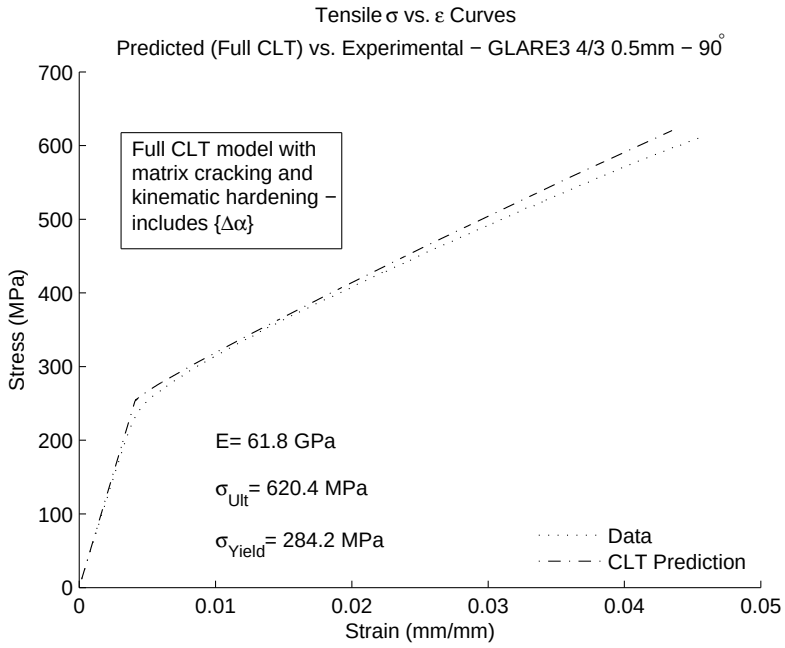

Figure 4.5 – *Full CLT Stress-Strain Prediction* - 90° *Specimen*

With the exception of the 0.4mm specimen, Figure **??**, the L and LT curves are fairly close to each other and the shape near yielding of the specimens in the rolling direction does not show a kink as yielding begins, showing a significantly smaller anisotropy than was modeled by Bouwman. For this reason, hardening data developed from this project was used for all calculations.

The effect of the movement of the yield surface was evaluated by varying the application of $\{\Delta\alpha\}$ term. There were three methods used to move the surface, with a constant radius. The first was to move the yield surface according to the method described in Equation 3.5. Alternatively, the evolution of the yield surface could be ignored, meaning that once a yield surface is crossed the next yield surface is activated and no additional yielding occurs until that yield surface is crossed, essentially assuming that $\{\Delta\alpha\} = \{0\}$. The final method is to assume that there is no offset, thus $\{\alpha\} = \{0\}$.

The predictions made using each of these methods are shown in Figures 4.10-4.14. The curves calculated using stiffness degradation due to plastic deformation and prepred damage as described previously are marked as "CLT Prediction - Best".

The prediction for the 0° specimen was made worse by addition of the kinematic shift due to movement of the yield surface, see Figure 4.10, while the prediction for the 90° specimen was improved with addition of the $\{\Delta\alpha\}$ term, see Figure 4.14. Predictions for 30°, 45°, and 60° show no discernible pattern with or without the kinematic shift

In the case where the yield surface stays centered at the origin in stress-space, $\{\alpha\} = \{0\}$. Predictions for on-axis tests were quite good, even compared to those developed using the $\{\alpha\}$ terms but without $\{\Delta\alpha\}$. This leads to the conclusion that in the direction of the fibers shifting of the yield surface is unnecessary. The reason is that in the direction of the fibers once yielding starts the stiffness of the laminate does not drop as precipitously as it does off-axis due to the direct loading of the fibers. The stiffness of the fibers means that load builds up extremely quickly in the laminate, thus the aluminum layers traverse very quickly through the yield surfaces and the effect of the offset is greatly decreased.

In general the predictions which used the full damage model without modifications were better than the predictions in which the kinematic shift of the yield surface was altered. Therefore the full

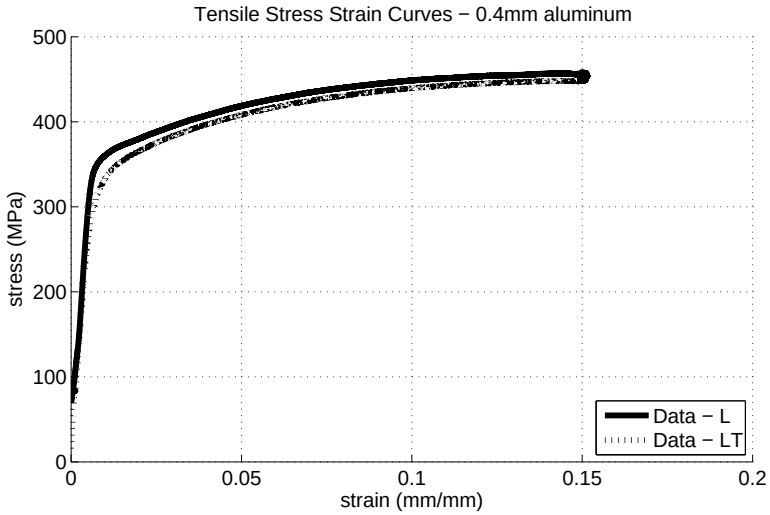

Figure 4.6 – *0.4mm Aluminum Stress-Strain Curve*

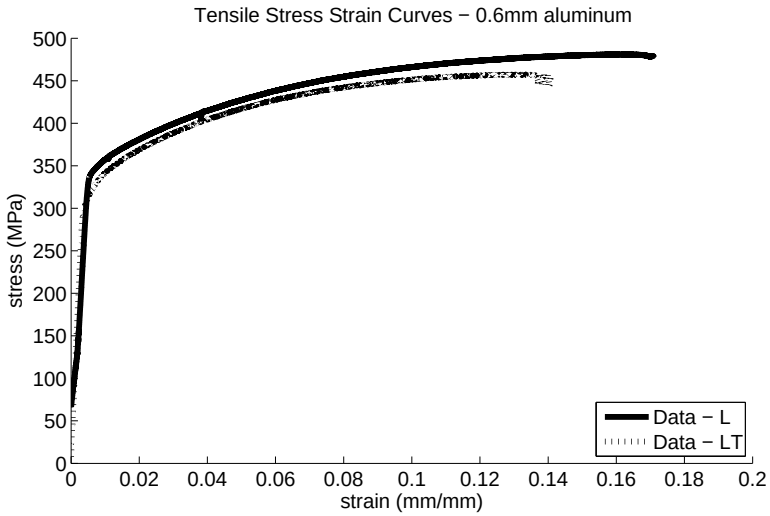

Figure 4.7 – *0.6mm Aluminum Stress-Strain Curve*

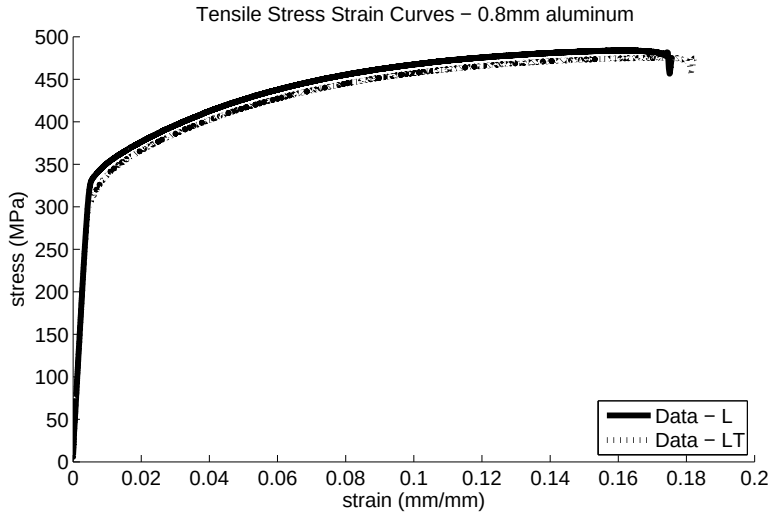

Figure 4.8 – *0.8mm Aluminum Stress-Strain Curve*

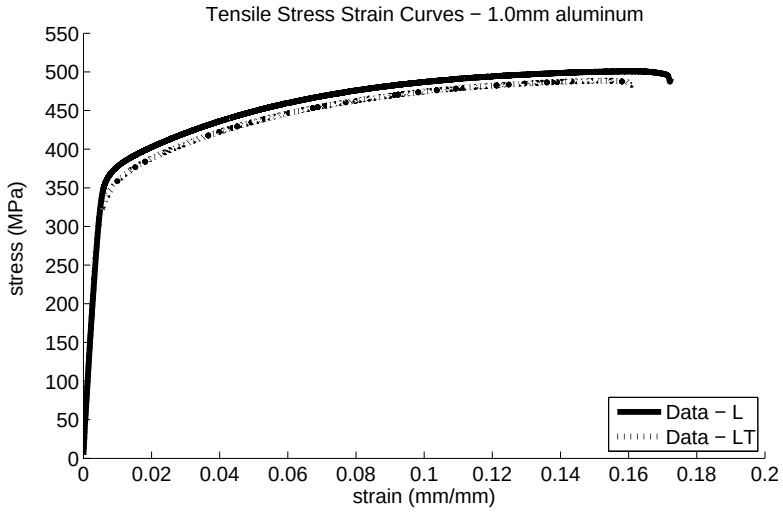

Figure 4.9 – *1.0mm Aluminum Stress-Strain Curve*

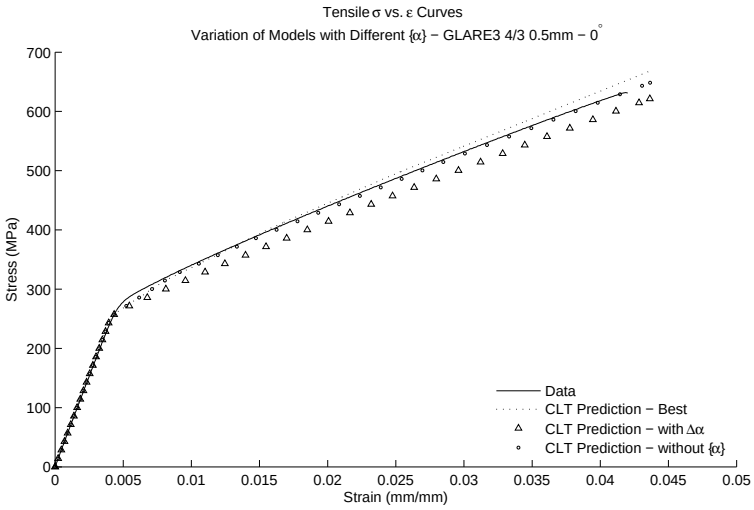

Figure 4.10 – *Full CLT Stress-Strain Prediction - 0° Specimen with different* $\{\alpha\}$

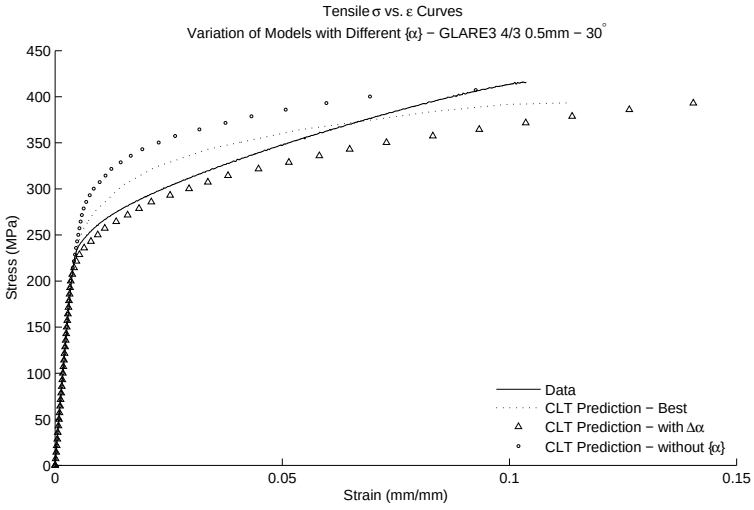

Figure 4.11 – *Full CLT Stress-Strain Prediction - 30° Specimen with different* $\{\alpha\}$

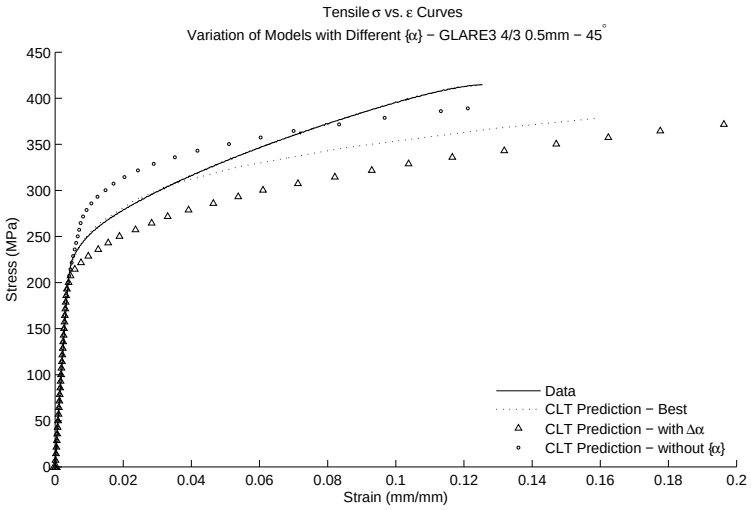

Figure 4.12 – *Full CLT Stress-Strain Prediction -* 45° *Specimen with different* $\{\alpha\}$

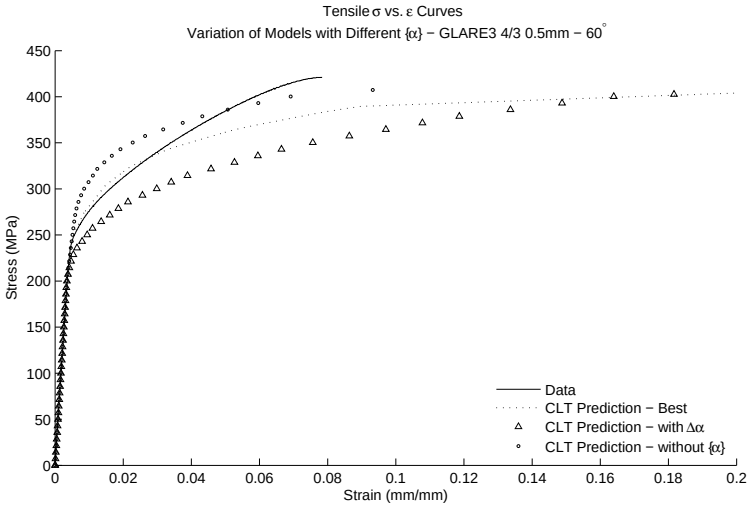

Figure 4.13 – *Full CLT Stress-Strain Prediction -* 60° *Specimen with different* $\{\alpha\}$

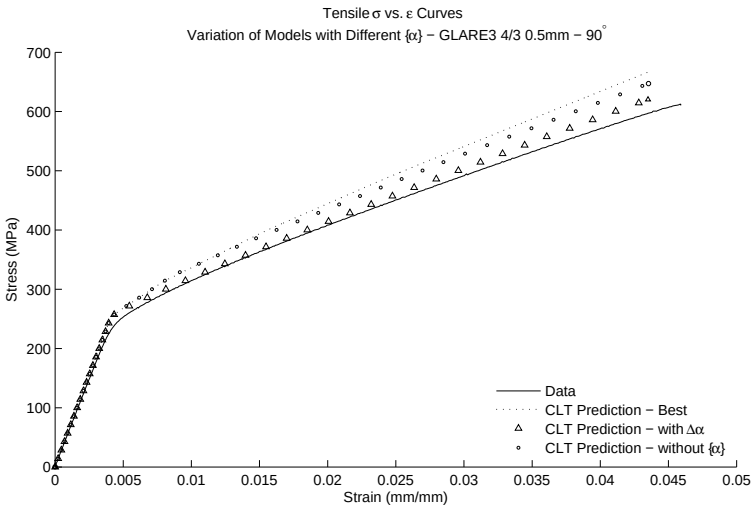

Figure 4.14 – *Full CLT Stress-Strain Prediction* - 90° *Specimen with different* $\{\alpha\}$

model is recommended for future use, and further research as described below.

4.2.2 Prepreg Damage Model

The damage evolution law used in this project was used as presented in the literature, but has not been specifically tested for FML sheets. Further testing would be required to determine whether damage occurs in FML sheets in the same pattern as in other fiber composite sheets. Because the matrix damage occurs at or below yielding of the metal constituent, the displacement relations between the sheets should not require any adjustment due to non-linear displacements. One parameter that needs to be determined is what the characteristic damage state of the matrix is in an FML. As was shown by Reifsnider[8], composite laminates reach a saturation point with regards to matrix crack density. It is possible that due to the incredibly high ductility of FML sheets that the matrix cracking in FML sheets continues until fracture instead of saturating at a stress-level below ultimate.

4.2.3 Shear Modeling

The Iosipescu shear test was used in this model to determine yield surface evolution via the kinematic shift in the shear stress direction. The question that should come to mind is whether the Iosipescu shear test accurately describes the behavior of the aluminum sheets which experience shear due to the orthotropic prepreg layers when loaded at an off-axis angle. When loaded at 30° near yielding the stress state in the laminate is $\sigma_1 =$ MPa, $\sigma_2 =$ MPa, and $\tau_{12} =$ MPa. This shear-dominated loading scenario raises the question whether the data used for the kinematic offset in the yield function is enough to accurately describe the yielding of the laminate in a shear-dominated loading scenario as will be experienced in FML sheets loaded off-axis. This question requires some additional research to determine whether the kinematic offset method captures shear yielding appropriately in this case. Perhaps the model is good, but could use a scaling factor on the yield strength term in the yield function, such as,

$$f = \sqrt{\overline{\sigma_x}^2 + \overline{\sigma_y}^2 + \overline{\sigma_x} \quad \overline{\sigma_y} + 3k_{12}\overline{\tau_{xy}}^2} - \sigma_Y = 0 \tag{4.1}$$

where k_{12} is some function of the loading angle in order to accurately model the shear-dominated loading.

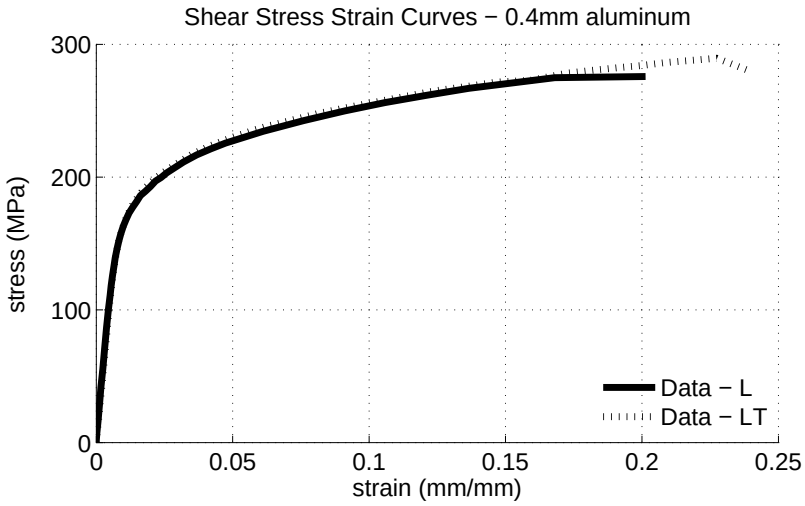

Figure 4.15 – *0.4mm Aluminum Shear Stress-Strain Curve*

A more fundamental question about the Iosipescu shear test is whether the shear stress-shear strain curve acquired from the test truly measures the property it is meant to measure. The assumption of pure shear in the area of the strain gage hinges upon perfect in-plane deformation of the specimen. It was beyond the scope of this project to evaluate the degree of out-of-plane deformation in the shear testing of the aluminum sheets, but the smoothness of the shear stress-shear strain curve, Figure 4.15, tends to lead to the conclusion that the testing through 20% strain could be assumed to accurately represent pure shear in the test section. In tensile loading the amount of imparted shear strain due to anisotropy of the FML sheets is far below the level where a different method for accounting for shear stress is required.

Chapter 5

Conclusions

The classical laminate theory in combination with the Ramberg-Osgood method for accounting for plastic deformation is a powerful tool for the determination of numerous static properties of fiber metal laminates. It makes accurate predictions possible to any designer, by performing a small number of simple tests on the metal thicknesses to be used in the FML. These simple tests provide the necessary constants and coefficients required to fully model the FML of interest in limited cases.

Despite the accuracy of the simple CLT/Ramberg-Osgood method in the fiber direction, this method immediately runs into limitations if the laminate is loaded in a direction other than aligned with the fibers. This limitation necessitates a more robust method, able to fully account for fibers oriented at angles other than 0° and 90° as well as plastic deformation at an angle other than the rolling or transverse directions of the metal sheets.

Various methods were investigated regarding the plastic deformation of the metal layers. Each of these methods was shown to be fairly accurate for tension curves by other researchers. The method used in this project uses a von Mises yield criterion and applies kinematic hardening to determine the stiffness of individual metal layers as loading increases.

The off-axis deformation properties of the prepreg layers were modeled by using equivalent constraint models where the layer of interest is explicitly modeled and the adjacent, constraining layers are modeled as equivalent, smeared layers. Using this method the degraded stiffness of the prepreg layer is found.

At each loading step the stiffness properties of individual layers are calculated. These individual stiffnesses are then combined using the standard CLT method, thereby providing the laminate stiffness matrix.

The method described in this report is a good first step in modelling generalized FML sheets at an arbitrary orientation. The model accurately predicts stress-strain curves on-axis, but still requires additional work to study the local interactions between metal and prepreg layers as damage occurs in each of those layers. The model described in this report assumes prepreg layers behave as they would when constrained by linear-elastic constraining layers, not the actual metal layers which show a large amount of plasticity during deformation in off-axis loading.

This report is a brief synopsis of a much larger research effort that will be published in full in Rickerd's thesis [13] to be submitted in the near future. Once complete, a copy of the thesis will be sent to EOARD.

Bibliography

[1] R. C. Alderliesten, M. Hagenbeek, J. J. Homan, P. A. Hooijmeijer, T. J. de Vries, and C. A. J. R. Vermeeren. Fatigue and damage tolerance of glare. *Applied Composite Materials*, 10(4):223–242, 2003.

[2] Thomas Beumler. *Flying GLARE*. PhD thesis, 2004.

[3] O. J. Bosker. Glare uni-axial blunt notch test results. Technical report, TU Delft, 2000.

[4] V. P. Bouwman. A calculation tool for structural analysis of general laminates. Technical report, NLR, 2002.

[5] Tjerk Johan de Vries. *Blunt and sharp notch behaviour of Glare laminates*. PhD thesis, 2001.

[6] J. Fan and J. Zhang. In-situ damage evolution and micro/macro transition for laminated composites. *Composites Science and Technology*, 47(2):107–118, 1993. Cited By (since 1996): 39 Export Date: 26 April 2012 Source: Scopus.

[7] M. Hagenbeek, C. v. Hengel, O. J. Bosker, and C. A. J. R. Vermeeren. Static properties of fibre metal laminates. *Applied Composite Materials*, 10(4-5):207–222, 2003.

[8] A.L. Highsmith and K.L. Reifsnider. *Stiffness-Reduction Mechanisms in Composite Materials*. Damage in Composite Materials: Basic Mechanisms, Accumulation, Tolerance, and Characterizations. ASTM, Bar Harbour, FL, 1982.

[9] J. J. Homan. Fatigue initiation in fibre metal laminates. *International Journal of Fatigue*, 28(4): 366–374, 2006.

[10] M. Kashtalyan and C. Soutis. Stiffness degradation in cross-ply laminates damaged by transverse cracking and splitting. *Composites Part A: Applied Science and Manufacturing*, 31(4):335–351, 2000.

[11] M. Kashtalyan and C. Soutis. Effect of delaminations induced by transverse cracks and splits on stiffness properties of composite laminates. *Composites Part A: Applied Science and Manufacturing*, 31(2):107–119, 2000.

[12] R.J. Nuismer and S.C. Tan. Constitutive relations of a cracked composite lamina. *Journal of Composite Materials*, 22(4):306–321, 1988.

[13] Gregory S Rickerd. *A Generic Static Model for Fiber Metal Laminates*. PhD thesis, 2013.

[14] G Roebroeks. The metal volume fraction approach. Technical report, TU Delft, 2000.

[15] G. H. J. J. Roebroeks. *Glare features*, chapter 2. Kluwer Academic Publishers, 2001.

[16] Geert Roebroeks. *Towards GLARE: The development of a fatigue insensitive and damage tolerant aircraft material*. PhD thesis, 1991.

[17] Jaap Schijve. *Fatigue of Structures and Materials*. Springer, 2nd edition, 2009.

[18] W. J. Slagter. On the bearing strength of fibre metal laminates. *Journal of Composite Materials*, 26(17):2542–2566, 1992.

[19] C. A. J. R. Vermeeren. *The Residual Strength of Fibre Metal Laminates*. PhD thesis, 1995.

[20] A. Vlot. *Historical overview*, chapter 1. Kluwer Academic Publishers, Dordrecht, Netherlands, 2001.

[21] Mao-Hong Yu, Guo-Wei Ma, Hong-Fu Qiang, and Yong-Qiang Zhang. *Generalized Plasticity*. Springer-Verlag, Berlin, 2006.

[22] J. Zhang and K. P. Herrmann. Stiffness degradation induced by multilayer intralaminar cracking in composite laminates. *Composites Part A: Applied Science and Manufacturing*, 30(5):683–706, 1999. Cited By (since 1996): 32 Export Date: 26 April 2012 Source: Scopus.

[23] J. Zhang, J. Fan, and K. P. Herrmann. Delaminations induced by constrained transverse cracking in symmetric composite laminates. *International Journal of Solids and Structures*, 36(6):813–846, 1999. Cited By (since 1996): 32 Export Date: 26 April 2012 Source: Scopus.

Chapter 6

Nomenclature

Symbols

$[Q]$	Lamina Stiffness Matrix
$[A]$	Laminate Extensional Stiffness Matrix
$[B]$	Laminate Extension-Bending Coupling Matrix
$[D]$	Laminate Bending Stiffness Matrix
t	Thickness

Acronyms

CLT Classical Laminate Theory

FEA Finite Element Analysis

FEM Finite Element Model

FML Fiber Metal Laminate

MVF Metal Volume Fraction

IDEF In-Situ Damage Effective Model